Session VIII, June 1, Thursday

L30

PRESENTATION OF LABORATORY OF X-RAY DIFFRACTOMETRY AND SPECTROMETRY, CENTRAL LABORATORIES, UCT PRAGUE

J. Maixner

Central Laboratories, University of Chemistry and Technology Prague, Technická 5, 166 28 Prague 6, Czech Republic

Central Laboratories at the University of Chemistry and Technology in Prague (https://clab.vscht.cz/) consists from nine laboratories and Laboratory of X-Ray Diffractometry and Spectrometry is one of them. The Central Laboratories were created with aim to provide support for scientific research and pedagogical activities of the faculties of the UCT Prague.

The main mission of laboratory consists in the determination of phase composition of samples using X-Ray diffraction analysis (XRD) involving the measurement and evaluation of diffraction patterns and in the determination of elemental composition of samples by X-ray fluorescence analysis (XRF). Samples are supplied from university departments but also from external customers.

XRD analysis are performed using the following instrumentation:

- D8 Advance diffractometer (Co tube), variable slits, transmission/reflective stage, sample changer, LynxEye 1D detector.
- X´Pert Pro diffractometer (Co tube), variable slits, transmission/reflective stage, sample changer and PIXcel1D detector.
- X'Pert^3 Powder diffractometer (Cu tube), variable slits, transmission/reflective stage, sample changer for 15 samples and PIXcel1D detector.
- Empyrean diffractometer (Cu tube), variable slits, eliptical mirror, transmission/reflective stage, sample changer for 45 samples, thin film attachment and PIXcel1D detector.
- D8 Discover microXRD diffractometer (Co tube), parallel polycapillary optics POLYCAP, 6 long collimators with inner diameter 0.05, 0.1, 0.3, 0.5, 1, 2 mm, motorized stage with XYZ range 0–24mm, VANTEC-500 2D X-ray detector
- The HTK 1200N chamber with furnace heater operating up to 1200 °C and MRI chamber with strip heater operating up to 1400 °C are available for in-situ X-ray diffraction studies in different atmospheres.
- The software package HIGHSCORE PLUS V 5.0e (PANalytical, Almelo, Netherlands) is used for data evaluation and search in databases PDF-4+2023 or PDF-4/Organics 2023.

XRF qualitative, semiquantitative and quantitative analysis are performed using the following instrumentation:

- Wavelength Dispersive fully automatic sequential spectrometers can measure 87 elements (Be-U, concentration from 1 ppm to 100%), sample must fit in cylindrical cassette, diameter 52mm and height up to 40mm. Samples are measured in vacuum.
- Possible samples – solid materials, powders and liquids.
- Axios WD spectrometer - Rh tube underneath sample, 4kW generator, 3 collimators, 6 masks (6, 10, 20, 27, 32, 37 mm), 8 crystals (PX1, PX5, PX4a, PX7, PE002, Ge 111, LiF 200, LiF 220), proportional and scintillation detectors. SuperQ sw is used to control spectrometr and for quantitative analysis. Omnian sw is used for standardless analysis in range F-U.
- Performix WD spectrometer - Rh tube underneath sample, 4.2kW generator, 4 collimators, 4 masks (1.5, 3, 15, 30 mm), 6 crystals (PE002, Ge 111, LiF 200, LiF 220, AX03, AX-BeB), proportional and scintillation detectors. Oxsas sw is used to control spectrometr, for quantitative analysis and mapping. Uniquant sw is used for standardless analysis in range F-U.
- ZSX Primus IV WD spectrometer - Rh tube above sample, 4kW generator, 3 collimators, 5 masks (0.5, 1, 10, 20, 30 mm), 6 crystals (PET 002-curved, Ge 111-curved, LiF 200, LiF 220, RX35, RX85), proportional and scintillation detector. ZSX sw is used to control spectrometr and for quantitative analysis. SQX software is used for standardless analysis in range B, F-U.
- Energy Dispersive spektrometer (Mg-U, 100ppm to 100%) :
- XL5 handheld ED spectrometer (Mg-U, 2 masks (3,8mm), concentration from 100ppm to 100%). Samples are measured in air, no limit on sample size. Standardless sw is not available = all elements in range Mg-U cannot be quantified simultaneously. Preinstalled calibration: General Metals (3,8mm) - 33 elements, Mining(8mm) - 41 elements, Plastics(8mm) - 24 elements, Soil(8mm) - 33 elements, Coating(3,8mm) - 30 elements. The report will include only elements in calibration.

L31

THE USE OF QM CALCULATION FOR STRUCTURE REFINEMENT - COMPARISON OF IAM AND HAR REFINEMENT RESULTS

M. Hušák, S. Chalupná

University of Chemistry and Technology, Prague, Technická 5, 166 28 Praha 6 – Dejvice
husakm@vscht.cz

Introduction

The most often used method for crystal structure refinement is based on Independent Atom Model (IAM). IAM gives identical atomic scattering factors for the same element under any situation ignoring the influence of the surrounding atoms. In reality the atomic scattering factors deepened on the actual electron shell configuration of the atom in the given position and given valence state. The issues with IAM can be handled by three methods: Multipole Model, Transferable Aspherical Atom Model (TAAM) [1] and Hirshfeld Atom Refinement (HAR) [2]. Multipole Model requires high-quality data and additional refinement parameters. TAAM model requires a precomputed database of atomic scattering factors for the given element with different surroundings. For TAAM the calculation can be done correctly only, when the parameters of the element under required configuration were already placed in the database. The recently introduced HAR refinement as implemented in Olex2 software [2] works with any sort of data and does not depend on atom scattering factor database. During HAR refinement the atomic scattering factors are calculated by external quantum mechanic (QM) software like e.g. Orca or Gaussian. The wave function generated by the QM code is than re-calculated in format suitable for the use for structure refinement. The QM code typically works with the molecule as with an isolated model in vacuum by the help of localized base. First test of combining the HAR refinement with modelling of the whole periodic system by plane waves and QM DFT calculation was already done as well [3].

The HAR refinement gives primary very different results for hydrogen atom positions. The results are closer to the hydrogen position obtained by neutron diffraction. The reason is a difference between the hydrogen nuclei position and the position of hydrogen related electron density maximum. From this reason we had chosen to test the HAR refinement futures on a salt-cocrystal continuum system for which characterization and proper determination of hydrogen positions is essential.

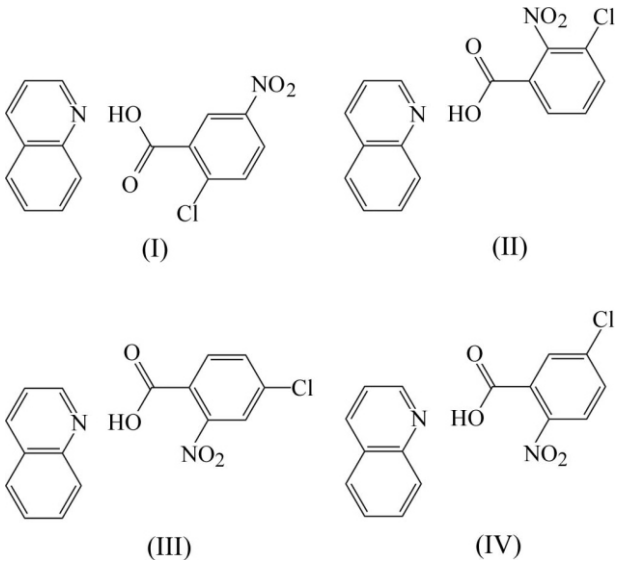

Figure 1. 2-chloro-5-nitrobenzoic acid–quinoline (1/1), (I) AJIWIA , 3-chloro-2-nitrobenzoic acid–quinoline (1/1), (II) AJIWOG, 4-chloro-2-nitrobenzoic acid–quinoline (1/1), (III) AJIWUM, and 5-chloro-nitrobenzoic acid–quinoline (1/1), (IV) AJIXAT.

For the IAM/HAR results comparison we had chosen a set of four quinoline isomeric compounds [4]. The studied structures formula, chemical names and CSD deposition codes are given in Fig. 1. For all these compounds a high-quality low temperature (185 K) Mo K data were already available. The system exhibits an interesting salt-cocrystal dynamic hydrogen transfer worth to study.

Methods

The original data from the authors were re-interpreted by the help of Olex2 software and HAR refinement by the NoSpheraA2 module [2]. Tree different refinement setups were used: 1) IAM with hydrogen atoms threaded isotropic 2) HAR with hydrogen atoms threaded isotropic 3) HAR with hydrogen atoms threaded anisotropic (disordered one

Table 1. Comparison of R factors for different refinement methods.

Refinement setup	I, AJIWIA	II, AJIWOG	III, AJIWUM	IV, AJIXAT
IAM original authors, SHELXL97	0.033	0.037	0.037	0.035
IAM re-refinement in Olex2	0.032	0.037	0.037	0.035
HAR re-refinement in Olex2	0.016	0.024	0.025	0.024
HAR re-refinement in Olex2, H-anisotropic	0.016	0.022	0.024	0.023

Table 2. Comparison of the hydrogen atom occupancy (salt N site) : (cocrystal O site)

Refinement setup	I, AJIWIA	II, AJIWOG	III, AJIWUM	IV, AJIXAT
IAM original authors, SHELXL97	0:1	0.39(3):0.61(3)	0.47(3):0.53(3)	0.65(3):0.35(3)
IAM re-refinement in Olex2	0.14(3):0.86(3)	0.25(3):0.75(3)	0.26(3):0.74(3)	0.61(3):0.39(3)
HAR re-refinement in Olex2	0.143(13):0.857(13)	0.19(2):0.81(2)	0.23(2):0.77(2)	0.62(2):0.38(2)
HAR re-refinement in Olex2, H-anisotropic	0.085(13):0.915(13)	0.18(3):0.82(3)	0.18(2):0.82(2)	0.51(6):0.49(6)

isotropic). The 1) and 2) refinement setup make possible to compare the R factor for situation with identical number of refined parameters. The QM calculations were done in Orca 5.0 software, cc-pVTZ base, PBE functional. To be able to model a disordered H positions the QM code had calculated for all structures models with hydrogen in both salt and cocrystal position. The refinement handled the structure as disordered between these two models. For all refinements the O-H and N-H distances of disordered hydrogen were restrained to get convergence.

Results

The results are summarized in Tab. 1 and Tab. 2.

The uses of HAR refinement significantly decrease the value of R factor. On the other hand, the uses of HAR refinement have only minor effect on the disordered hydrogen occupancy factor. For II and III a slight occupancy decrease in NH position can be observed probably due to including the nitrogen lone pair in the calculation. There is no significant change in R factor nor in occupancy for the refinement with hydrogen treated anisotropic in comparison to isotopic treatment.

The difference between IAM and HAR refinement and IAM refinement is even more visible on Fig. 2. The IAM refinement indicates hydrogen in 2 positions. The HAR refinement electron density map corresponds more close to the Path Integral Molecular Dynamic (PIMD) simulation results as calculated for similar situations [5]. The hydrogen is not exactly in 2 positions but instead creates a disordered cloud of electrons between the oxygen and hydrogen atoms.

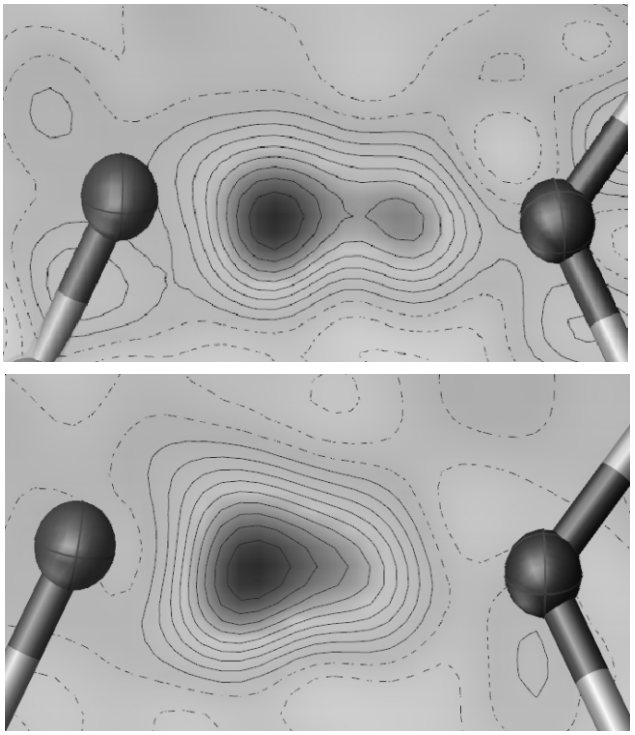

Figure 2. Difference electron density calculation for AJIWUM in the O…H…N region. IAM refinement (upper) and HAR refinement (H treated anisotropic) (lower).

1. W. F. Sanjuan-Szklarz, et. al., *IUCrJ*, **3**, (2016), 61.
2. F. Kleemiss, et. al., *Chem. Sci..*, **12**, (2021), 1675.
3. P. N. Ruth, M. R. Herbst-Irmer, D. Stalke, *IUCrJ*, **9**, (2022), 286.
4. K. Gotoh, H. Ishida, *Acta Cryst.*, C**65**, (2009), o534.
5. J. R. Štoček, et. al, *J. Am.Che,. Soc.,* **144**, (2022), 711.

L32

INVESTIGATION OF PHASES FROM SALT-COCRYSTAL CONTINUUM USING DFT CALCULATIONS

S. Chalupná (maiden name Šajbanová), **M. Hušák**

Department of Solid State Chemistry, University of Chemistry and Technology, Prague, Technická 5, Praha 6, 166 28, Czech Republic

sajbanos@vscht.cz

Introduction

A broad range of solid forms available for pharmaceutical molecules exists nowadays. Pharmaceutical salts are one of the forms that can be used for formulation of active components. About 50% of drugs used today are salts. Additionally, cocrystals are rapidly evolving as another prominent type of pharmaceutical form. [1,2] The difference between salt and cocrystal is given only by the position of single hydrogen. As this difference is quite small, it is an essential task to develop new techniques that can accurately identify the precise location of the relevant hydrogen atom. We had already developed and partially tested a computational method for salt cocrystal differentiation based on DFT energy calculation. [1,3]

The DFT method optimizes an artificially constructed wrong structure (hydrogen atom placed in salt position near the potential acceptor for cocrystals and vice versa cocrystal position with hydrogen atom placed near the potential donor of the salts). The verification of the method was done based on comparison of the results with an experimentally confirmed correct hydrogen position on 95 structures. As the data source for testing of the DFT method we used a Cambridge Structural Database (CSD) deposition code list of structures from the zone (-1 *pKa* 4), defined in an article "Acid–base crystalline complexes and the pKa rule". [4]

In addition to the salt and cocrystal form, we had detected presence of a form which can be described as salt-cocrystal continuum. For such a form the hydrogen can be found in two energetic minima (Fig. 1). The detection and examination of these forms is crucial for ensuring compliance with legal and regulatory standards.

In addition, a quantum dynamic simulation was performed to verify that the results of the DFT method correspond to the room temperature state of the crystals.

Methods

The DFT method uses the newest version of Castep 22.11 software. The rSCAN functional in combination with MBD dispersion correction and fine basis precision was used. The data were prepared in BIOVIA Materials Studio software. Computation was performed on Karolina supercomputer at TU Ostrava. The computational power required for calculation of 450 structures was approximately 3 000 core/hours on 128 core nodes.

In addition to simple geometry optimization, we had performed Path Integral Molecular Dynamics (PIMD) simulation for one structure (CSD code AJIWUM). PIMD is a computational simulation method that combines Molecular Dynamics (MD) and description of Nuclear Quantum Effects (NQE). We have used quantum PIMD simulation because the energy was calculated by DFT method. The Path Integral (PI) involves representing the motion of particles as a path of imaginary time slices, which allows the inclusion of NQE effects in MD. PIMD is particularly useful in studying systems with strong NQE effects, such as hydrogen bonding or proton transfer. [5] The PIMD simulation of the studied system was also performed in CASTEP. NVT ensemble, temperature of 150 K, a Langevin thermostat, a 0,5-fs integration time step and a planewave cut-off energy of 571 eV were used. For energy calculation we had used rSCAN functional with MBD dispersion correction again. The path-integral propagation used a Trotter decomposition of all nuclei into 16 beads, which has been shown

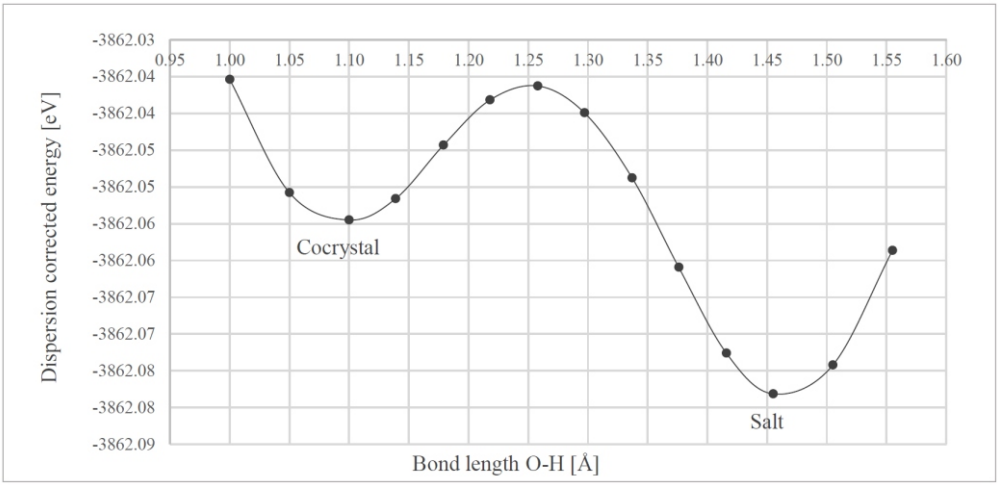

Figure 1. Energy dependence on H atom position for the PUJNIS structure calculated by the PBE+TS functional [1]

Table 1. Results of calculation on 418 structures from the zone with (-1 *pKa* 4) (RSCAN fine + MBD).

Pure cocrystal	Pure salt	Salt-cocrystal continuum phase
312	16	90

Table 2. Results of calculation on 30 structures with experimentally detected salt-cocrystal disordered hydrogen (RSCAN fine + MBD) .

Pure cocrystal or solvate	Pure salt	Confirmed salt-cocrystal continuum phase
7	7	16

to be sufficient for simulations of molecular crystals at 300 K. [6]

Results

The results of structures from the zone (-1 *pKa* 4) are summarized in Tab.1. While testing our computational method, we discovered 90 structures that exhibit the above-mentioned two energetic minima. Further investigation of these structures is yet to be conducted.

An additional 30 structures with dual hydrogen position were detected using the 3D search for disordered hydrogen position. In this study we had investigated both salts, cocrystals and solvates. For these structures, the presence of a double hydrogen position had already been detected by the original authors. We proceeded to perform DFT calculations on these structures, using the settings specified above. The results are summarized in Tab. 2.

As a sample of structure described incorrectly based on experiment, we can mention structure with CSD deposition code ILUCIB. It was identified by us as a pure solvate, which differs from the classification given in the original publication. This structure is composed of pyridinium (*pKa* = 5,23) and 3,3',4-tri-O-methylflavellagate (*pKa* 6). [7] That means that $pKa = pK_a[\text{base}] - pK_a[\text{acid}] = 1$, but actual flavonoid salts are formed when *pKa* is approximately 10. [7] Therefore, we believe that the structure is incorrectly solved, and it cannot be a salt or salt-cocrystal continuum phase. Other incorrect results will be evaluated using the same approach.

For structure with CSD deposition code AJIWUM the Path Integral Molecular Dynamic (PIMD) simulation was performed. In Figure 2 we can see the probability distribution of the N H (or N…H) distance in AJIWUM system. Results of this simulation reveal that the hydrogen is not precisely located in 2 positions but is delocalized between the donor and the acceptor of the H-bond. Such situation will be probably common for most structures from the salt-cocrystal continuum area at room temperature.

1. Šajbanová, S. *Validace metody rozlišení solí a kokrystalů pomocí DFT výpočtu*. diplomová práce, Vysoká škola chemicko-technologická v Praze, červen 2022.
2. Kratochvíl, B. KOKRYSTALY A JEJICH OČEKÁVANÉ FARMACEUTICKÉ APLIKACE. *Chem. Listy* 2010, 104, 823–830.
3. Hušák, M.; Šajbanová, S.; Klimeš, J.; Jegorov, A. The possibilities of salt-cocrystal distinguishing based on dispersion-corrected density functional theory calculations. *Acta Crystallographica Section B.* 2022, 78, 5, 781 – 788.
4. Cruz-Cabeza, A. J. Acid–base crystalline complexes and the pKa rule. *CrystEngComm* 2012, 14, 6362–6365.
5. R. P. Feynman and A. R. Hibbs, Quantum Mechanics and Path Integrals (McGraw-Hill, New York, 1965).
6. Štoček JR, Socha O, Císařová I, Slanina T, Dračínský M. Importance of Nuclear Quantum Effects for Molecular Cocrystals with Short Hydrogen Bonds. *J Am Chem Soc*. 2022 Apr 27;144(16):7111-7116. doi: 10.1021/jacs.1c10885. Epub 2022 Apr 8. PMID: 35394771.
7. Elisabet Fuguet, Clara Rŕfols, Meritxell Mańé, Rebeca Ruiz, Elisabeth Bosch, Acidity constants of hydroxyl groups placed in several flavonoids: Two flavanones, two flavones and five flavonols,*Talanta*,Volume 253,2023,124096,ISSN 0039-9140,https://doi.org/10.1016/j.talanta.2022.124096.

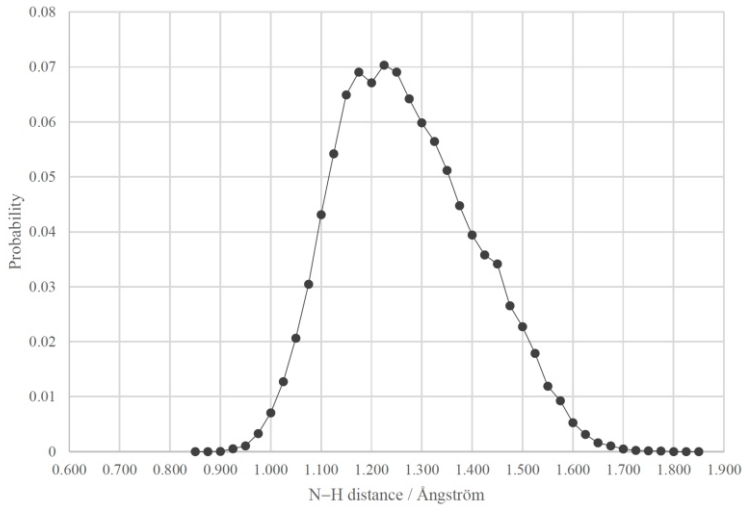

Figure 2. Probability distribution of the N–H distances obtained from PIMD simulation of AJIWUM

L33

BENCHMARKING HIRSHFELD ATOM REFINEMENT – APPLICATION OF ECP FOR RELATIVISTIC SYSTEMS

Y. R. Pateda

Comenius University in Bratislava, Faculty of Natural Sciences, Department of Inorganic Chemistry, Mlynská dolina, Ilkovičova 6, 842 15 Bratislava, Slovak Republic

rao2@uniba.sk

Hirshfeld/Generalized Atom Refinement (HAR/GAR) [1] allows to calculate individually tailored aspherical scattering factors (pseudoatoms) by using *Olex2* [2] and *NoSpherA2* [3] software together with quantum chemical packages like *Orca* [4] or *Tonto* [5]. However, the choice of the electron density calculation method is usually experience based. With a high-quality data, using a large basis set with the functionals from the top of the "Jacob's Ladder" [6] can be meaningful. In [7] and [8], we did some benchmarking of HAR methods using *Orca* version 4.2.1 and 5.0.3 with the $NH_4[Zn(cma)(H_2O)_2]\cdot H_2O$ data suffering from suboptimal absorption correction. This work is dedicated to the HAR refinement of relativistic systems by ECP based methods using *Orca* 5.0.4.

As a starting point for HAR, the results of the IAM refinement of selected compounds using proper constraints with X–H distances free to refine were used. The refinements for all combinations of selected LDA (PWLDA), GGA (BLYP, PBE), meta-GGA (TPSS, R2SCAN), hybrid GGA (B3LYP, PBE0), hybrid meta-GGA (M06-2X) and range separated hybrid (B97X) functionals with ECP-def2-SVP – def2-TZVPP basis sets were performed by *Olex2 1.5* in combination with *NoSpherA2* and *Orca 5.0.3*. For the comparison, calculations using all-electron x2c-def2-TZVP basis set with R2SCAN functional with ZORA approximation were also performed. The results were compared with previous results in [8] and with the values obtained from neutron diffraction [9].

Regarding the time of calculation, the functionals were divided into two groups. LDA, GGA and meta-GGA functionals were significantly faster than hybrids, with meta-GGA hybrids and range separated hybrids being slower than GGA hybrids.

Similarly to [8], if the data were influenced by strong absorption effect, PWLDA is best all-round performer (except of ECP-def2-TZVP/R2SCAN combination), followed by R2SCAN and M06–2X and PBE0 being on par, with the best results using ECP-def2-TZVP basis set. Otherwise, the results are better when using larger basis sets and the best performer is PBE0 functional followed by PBE and B97X or R2SCAN. Residuals (*R*, w*R*, *S*) were practically identical for all refinement methods.

For individual bond types, there are often best performing basis set/functional combinations. Agreement between obtained distances and neutron defaults was exceptionally good for $C–Csp^3–H_3$ and $C_{ar}–H$ distances. Although there is no reference for $(C_{ar})_2–Nsp^3–H$ (N pyramidal) distance based on neutron data, but we found $C_{ar}–N–H_2$ (N pyramidal) distance [9] being in a good agreement with refined distance.

Non-empirical GGA and GGA hybrid functionals (PBE, PBE0) outperformed empirical (BLYP, B3LYP) GGA and GGA hybrids by a small margin. Using all-electron x2c-TZVP/R2SCAN method using ZORA approximation didn't led to significantly different results with approximately the same calculation times.

1. M. L. Chodkiewicz, M. Woińska and K. Woźniak, *IUCrJ*, **7**, (2020), 1199–1215.
2. L. J. Bourhis, O. V. Dolomanov, R. J. Gildea, J. a. K. Howard and H. Puschmann, *Acta Crystallogr. Sect. A Found. Adv.*, **71**, (2015), 59–75.
3. F. Kleemiss, O. V. Dolomanov, M. Bodensteiner, N. Peyerimhoff, L. Midgley, L. J. Bourhis, A. Genoni, L. A. Malaspina, D. Jayatilaka, J. L. Spencer, F. White, B. Grundkötter-Stock, S. Steinhauer, D. Lentz, H. Puschmann and S. Grabowsky, *Chem. Sci.*, **12**, (2021), 1675–1692.
4. F. Neese, *Wiley Interdiscip. Rev. Comput. Mol. Sci.*, **12**, (2022), 1–15.
5. D. Jayatilaka and D. J. Grimwood, *Lect. Notes Comput. Sci. (including Subser. Lect. Notes Artif. Intell. Lect. Notes Bioinformatics)*, **2660**, (2003), 142–151.
6. S. F. Sousa, P. A. Fernandes and M. J. Ramos, *J. Phys. Chem. A*, **111**, (2007), 10439–10452.
7. J. Chrappová, Y. R. Pateda and E. Rakovský, *J. Chem. Crystallogr.*, **53**, (2023), 228–235.
8. Y. R. Pateda and E. Rakovský, in *24. celoslovenská študentská vedecká konferencia s medzinárodnou účas ou 23.11.2022, Chémia a technológie pre život, FCHPT STU*, edited by M. Reháková & J. Oravec, (Bratislava: Slovenská chemická knižnica), 2022, pp. 93–94.
9. F. H. Allen and I. J. Bruno, *Acta Crystallogr. Sect. B Struct. Sci.*, **66**, (2010), 380–386.

This work was supported by the Operation Program of Integrated Infrastructure for the project, UpScale of Comenius University Capacities and Competence in Research, Development and Innovation, ITMS2014+: 313021BUZ3, co-financed by the European Regional Development Fund.

L34

MOLECULAR SIMULATION OF INTERACTIONS BETWEEN PALYGORSKITE AND TiO_2

Miroslav Pospíšil[1], Aristos Mavrikos[2], Eleni Gianni[2], Christina-Vasiliki Lazaratou[2], Milan Pšenička[1] and Dimitrios Papoulis[2]

[1]Charles University, Faculty of Mathematics and Physics, Ke Karlovu 3, Prague 2, 12116, Czechia
[2]Department of Geology, University of Patras, Rio, 26504 Patras, Greece
miroslav.pospisil@mff.cuni.cz

TiO_2 is very often used for photocatalytic applications because it is widely available, cheap and environmentally friendly photocatalytic material. Nevertheless, the anatase (preferred crystal structure) nanoparticles have tendency to agglomerate and this process causes a significant decreasing in catalysis efficiency. To avoid the agglomeration, we used the fibrous clay minerals such as palygorskite to anchor TiO_2 particles among its fibres. This causes the photocatalytic properties of small nanoparticles to be preserved and no agglomeration due to the strong mutual interactions between TiO_2 and clay fibres.

Palygorskite–TiO_2 nanocomposites were prepared and characterized by various experimental techniques (X-ray diffraction, Fourier transform-infrared spectroscopy and transmission electron microscopy) in Greece, while their mutual interactions including probable spontaneous bonding between clay and TiO_2 spheres were calculated by molecular simulation methods. Three different palygorskite supercells were built with different type of surface with the largest amount of oxygen atoms, see Figure 1, which were subsequently calculated in various positions with the TiO_2 spheres with suitable adjacent surfaces, see Figure 2.

A monoclinic palygorskite structure was used for the calculations, the unit cell parameters of the crystal structure were as follows: $a = 13.337$ Å, $b = 17.879$ Å, $c = 5.264$ Å, $= = 90°$ and $= 105.270°$, space group *C2/m* [2, 3]. An optimized crystal structure of TiO_2, in the form of anatase, was imported from Materials Studio database with the following cell parameters: $a = 3.776$ Å, $b = 3.776$ Å, $c = 9.486$ Å, $= = = 90°$, and the space group number 141 and type *I41/amd*. A supercell of anatase was created with the following parameters: A = 20 *a*, B = 20 *b*, C = 10 *c*.

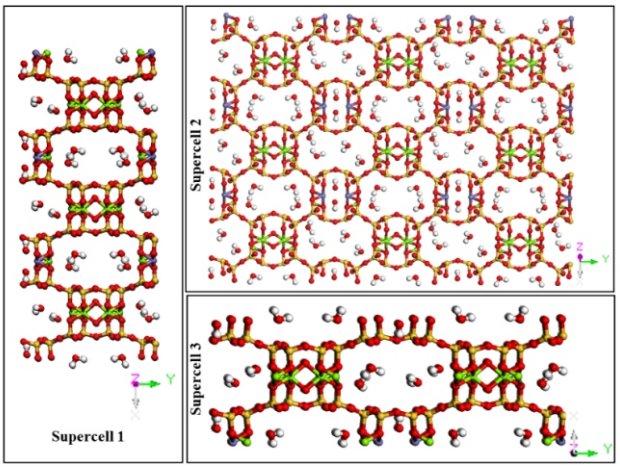

Figure 1. The three supercells under different point of view. Supercell P1: A = 3, B = 1, C = 7 Supercell P2: A = 3, B = 3, C = 1 Supercell P3: A = 1, B = 2 and C = 7 [1].

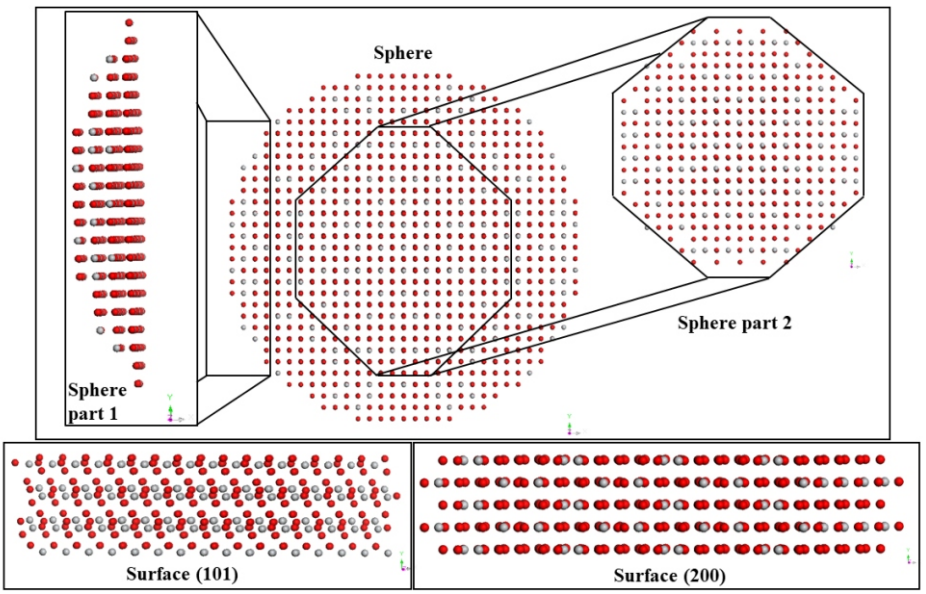

Figure 2. The anatase (i) sphere part 1 and 101 and (ii) sphere part 2 and 2i the parts of anatase that were combined with palygorskite surface [1].

The simulations showed that optimal TiO_2-palygorskite connection takes place among the Ti atoms of the curved TiO_2 part of sphere with the O atoms of the P1 surface of palygorskite through strong electrostatic interactions and the possible formation of covalent bonds due to the short distance between the surfaces, see Table 1. Due to the simulation, we can see the detailed curved part of anatase with Ti atoms which closely interacting and nearly connected to the O atoms on various surfaces of palygorskite [1].

Table 1. Three shortest Ti-O distances of the selected optimized models [Å].

Name	Distance 1	Distance 2	Distance 3
P11	2.748	2.909	3.143
P1101	2.123	2.185	2.198
P12	1.800	1.814	1.872
P12i	1.790	2.050	2.627

1. A. Mavrikos, M. Pospíšil, E. Gianni, C. V. Lazaratou, M. Pšenička, D. Papoulis, Interactions among TiO_2 and palygorskite revealed: Boost for stability of well-known photocatalyst, *Journal of Molecular Liquids*, **343**, (2021), 117678.

2. R. Giustetto, R., Chiari, G.: *Eur. J. Mineral.*, 16, (2004), 521–532.

3. C. V. Lazaratou, D. Panagiotaras, G. Panagopoulos, M. Pospíšil, D. Papoulis, *Environ. Technol. Innov.*, **19**, (2020), 100961.

L35

VLIV DLOUHODOBÉHO PŘIROZENÉHO STÁRNUTÍ NA STRUKTURU iPB-1 A RYCHLOST PŘEMĚNY FÁZE II – I

Kaszonyiová M.[1]*, Rybnikář F.[1], Lapčik L.[2], J. Vilčáková[3]

[1]Department of Polymer Engineering, Tomas Bata University in Zlin, 760 01, Czech Republic
[2] Department of Food Technology, Tomas Bata University in Zlin, 760 01, Czech Republic
[3]Centre of Polymer Systems, Tomas Bata University in Zlín, 760 01, Zlín, Czech Republic
**for correspondence, e-mail: mhribova@utb.cz, address: Department of Polymer Engineering, Faculty of Technology, Tomas Bata University in Zlin, Vavreckova 275, 760 01, Czech Republic*

Isotaktický polybuten-1 (iPB-1) je termoplastický polymer s vysokou krystalinitou a vynikajícími fyzikálními vlastnostmi, což z něj dělá ideální materiál pro výrobu různých výrobků, jako jsou například trubky, obaly kabelů, vodovodní potrubí a další. Tyto pozoruhodné vlastnosti jsou nepříznivě ovlivněny pomalou přeměnou původní fáze II na stabilní fázi I, která sice zlepšuje vlastnosti, ale zároveň je spojena se smršťováním o 4 % v důsledku rozdílných hodnot hustoty obou fází. Dále, jak se ukazuje, iPB-1 podléhá přirozenému stárnutí, což může ovlivnit jeho fyzikální a mechanické vlastnosti.

Studie dlouhodobého přirozeného stárnutí vzorků iPB-1 s různou molekulovou hmotností ukázala, že rychlost transformace z počáteční fáze II do stabilní fáze I se výrazně snižovala s časem stárnutí trvajícím až 17 let. Celková krystalinita se s časem stárnutí také snižovala a malé množství fáze II zůstávalo nestabilní po dobu minimálně 17 let. Vzorek s nižší molekulovou hmotností (DP 0400) vykazoval vyšší rychlost fázové transformace II na I než vzorek PB 0110, dokonce i po opakovaném tavení polymeru a jeho nové krystalizaci.

Hlavním fenoménem stárnutí iPB-1 je pravděpodobně změna poměru funkčních skupin methyl/methylen, která může být způsobena štěpením vedlejších řetězců. Tento proces snižuje geometrickou pravidelnost molekulového řetězce a zpomaluje postupující fázovou transformaci II na I. Předpokládá se, že separace vedlejších řetězců také vede k tvorbě skupin, které dále zpomalují fázovou transformaci, ale tyto skupiny mohou být odstraněny opakovaným tavením vzorku.

Tyto výsledky jsou důležité pro průmyslové aplikace iPB-1, protože ukazují, že přirozené stárnutí může ovlivnit jeho fyzikální a mechanické vlastnosti.

1. KASZONYIOVÁ, M., F. RYBNIKÁŘ, L. LAPČÍK a J. VILČÁKOVÁ. The effect of long-term natural aging on the iPB-1 structure and the II – I phase transformation rate. Polymer Degradation and Stability. 2021, 183. ISSN 01413910. Doi:10.1016/j.polymdegradstab.2020.109437.

2. BENÍČEK, L., L.CHVÁTALOVÁ, M. OBADAL, R. ČERMÁK, V. VERNEY and S. COMMEREUC. Photo-degradation of isotactic poly(1-butene): Multiscale characterization. Polymer Degradation and Stability. 2011, 96(10), 1740-1744. DOI: 10.1016/j.polymdegradstab.2011.08.001.

3. CHANDRA, R. Review of investigations on degradation and stabilization of poly(1-butene). Progress in Polymer Science. 1985, 11(1-2), 23-27. DOI: 10.1016/0079-6700(85)90006-1.

4. BIGG, D. M., K. J. HEATER, B. L. GRUNDEN, D. E. BADOWSKI, J. G. RICKS and J. BRASCH. Analysis of the degradation of poly(1-butene) pipe through oxidation induction time tests. Advances in Polymer Technology. 2005, 24(3), 215-225. DOI: 10.1002/adv.20045.

5. SHAO, H., S. WANG, D.JIANG and A. HE. Effect of Antioxidant System on Aging Properties of Poly(1-butene) and the Aging Mechanism. Journal of Macromolecular Science, Part B. 2016, 55(7), 643-651. DOI: 10.1080/00222348.2016.1186526.

6. SUN, B., L.CUI, X. JIANG, B. JIANG, W. YAO and A. HE. Influence of catalyst residues on thermo-oxidative aging and thermal stability of poly(butene-1). Chinese Journal

of Polymer Science. 2014, 32(5), 633-639. DOI: 10.1007/s10118-014-1433-x.

7. SINGH, R. P. and A. SYAMAL. Effect of copper (II) chelate on photo-degradation of poly (1-butene). Journal of Materials Science [online]. 1981, 16(12), 3324-3330 [cit. 2020-07-07]. DOI: 10.1007/BF00586293.

8. SINGH, R.P. Kinetics of photo-sensitized and photo-stabilized photo-degradation of isotactic poly(1-butene). Polymer Degradation and Stability [online]. 1985, 13(4), 313-326 [cit. 2020-07-07]. DOI: 10.1016/0141-3910(85)90080-1.

9. CHANDRA, R. Thermal and photo-oxidative degradation of poly-1-butene film in the presence of zinc thiopicoline anilide. Journal of Applied Polymer Science [online]. 26(8), 2509-2518 [cit. 2020-07-07]. DOI: 10.1002/app.1981.070260802.

L36

CRYSTAL STRUCTURE MODIFICATIONS IN ORGANIC CHARGE-TRANSFER SALT – -$[(BEDT\text{-}TTF)_{1-x}(BEDT\text{-}STF)_x]_2Cu_2(CN)_3$

Petr Doležal

Matematicko-fyzikální fakulta UK, Ke Karlovu 5, 121 16 Praha 2

-$[(BEDT\text{-}TTF)_{1-x}(BEDT\text{-}STF)_x]_2Cu_2(CN)_3$ series are 2D organic salts realizing a paradigmatic Mott-metal insulator transition. The localization of conduction electrons is driven by strong electronic correlations which can be tuned by hydrostatic pressure or by substitution with BEDT-STF cations as in the present study. The parent -$(BEDT\text{-}TTF)_2Cu_2(CN)_3$ compound remains without magnetic ordering down to the lowest temperatures. To fully understand its magnetic properties it is necessary to assess its crystal structure in detail. The (BEDT-TTF) cations are separated by the layers of $Cu_2(CN)_3$ anions within in the ***bc*** plane, see figure below. If one looks on the cations along ***a*** crystallographic axis it is possible to see the triangular arrangement of $(BEDT\text{-}TTF)_2$ dimers, see panel (b) below. The triangular lattice is close to ideal, $t/t' = 0.83$, providing ideal conditions for geometrical frustration [1]. Each dimer is carrying one electron with spin S = 1/2. The interaction between spins is antiferromagnetic [2]. These all are necessary conditions for the formation of quantum spin liquid (QSL) sate and also the reason why this compound was the prime QSL candidate. The observation of $T^* = 6$ K anomaly in thermal expansion brought the question about the proper ground state, which seems to be rather a valence bond solid (VBS) than QSL [3]. This leads to the more general question whether geometrical frustration on its own can fully suppress antiferromagnetic order and whether the systems can truly remain stable towards magneto-structural instabilities, like VBS phases, down to absolute zero.

Our presented contribution is focused on low temperature X-ray diffraction study of a single crystalline sample -$(BEDT\text{-}TTF)_2Cu_2(CN)_3$, showing pronounced anomaly of lattice parameters around $T^* = 6$ K. The structural results are supplemented by a microscopic study using nuclear magnetic resonance (NMR).

This work was supported by the Czech Science Foundation under Grant No. 23-06810O.

1. H. C. Kandpal, I. Opahle, Y.-Z. Zhang et al., *Phys. Rev. Lett.* **103** (2009) 67004.

2. Y. Shimizu, K. Miyagawa, K. Kanoda et al., *Phys. Rev. Lett.* **91** (2003) 107001.

3. B. Miksch, A. Pustogow, M. J. Rahim et al., *Science* **372** (2021) 276-279.

4. A. Pustogow, Solids **3** (2022) 93-110.

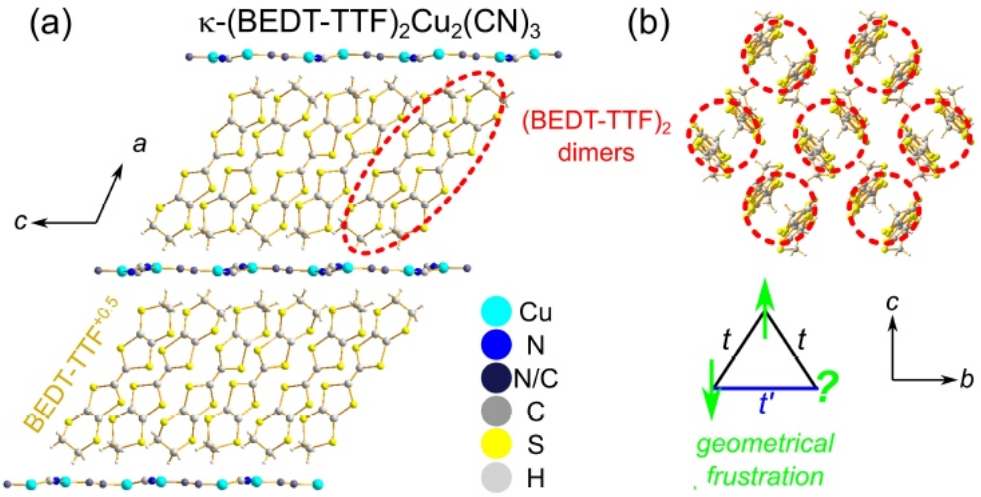

Figure 1. Crystal structure of -$(BEDT\text{-}TTF)_2Cu_2(CN)_3$ 2D organic salt. a) View along ***b*** axis. b) The arrangement of dimers within ***bc*** plane. Taken from [4].